Mineralogy of volcanic rocks in Gusev Crater, Mars: Reconciling Mössbauer, Alpha Particle X-Ray Spectrometer, and Miniature Thermal Emission Spectrometer spectra

H. Y. McSween,[1] S. W. Ruff,[2] R. V. Morris,[3] R. Gellert,[4] G. Klingelhöfer,[5] P. R. Christensen,[2] T. J. McCoy,[6] A. Ghosh,[1] J. M. Moersch,[1] B. A. Cohen,[7] A. D. Rogers,[8] C. Schröder,[5] S. W. Squyres,[9] J. Crisp,[10] and A. Yen[10]

Received 20 July 2007; revised 28 October 2007; accepted 23 January 2008; published 29 May 2008.

[1] Complete sets of mineral abundances for relatively unaltered volcanic or volcaniclastic rocks in Gusev Crater have been determined by modeling Mössbauer subspectral areas as mineral weight percentages, and combining those percentages with the proportions of iron-free minerals not detected by Mössbauer (normative plagioclase, apatite, and chromite, as calculated from Alpha Particle X-Ray Spectrometer (APXS) chemical analyses). Comparisons of synthetic thermal emission spectra calculated for these mineral modes with measured Miniature Thermal Emission Spectrometer (Mini-TES) spectra for the same rock classes show either good agreements or discrepancies that we attribute to sodic plagioclase compositions or unmodeled sulfate, glass, or pigeonite. The normative compositions of olivine, pyroxene, and feldspar calculated from APXS data are consistent with spectroscopic constraints on mineral compositions. Systematic variations between olivine abundances in APXS norms (which sample tens of micrometers depth) and olivine proportions measured by Mössbauer (which sample hundreds of micrometers depth) support the hypothesis that dissolution of olivine by acidic fluids has occurred on weathered rock surfaces.

Citation: McSween, H. Y., et al. (2008), Mineralogy of volcanic rocks in Gusev Crater, Mars: Reconciling Mössbauer, Alpha Particle X-Ray Spectrometer, and Miniature Thermal Emission Spectrometer spectra, *J. Geophys. Res.*, *113*, E06S04, doi:10.1029/2007JE002970.

1. Introduction

[2] Decades of spectroscopic measurements from Earth-based telescopes and orbiting spacecraft have revealed clues about the mineralogy of the Martian surface, but determining the mineralogy of Mars rocks has remained a challenge. Many diagnostic visible/near-infrared (VNIR) spectral features are masked by nanophase iron oxides in the ubiquitous dust covering much of the planet's surface [*Bell et al.*, 2000], and thermal infrared (TIR) spectra are compromised by volume scattering and nonlinear mixing in dust-covered regions, as well as by atmospheric obscuration [*Christensen et al.*, 2001]. For less dusty areas, deconvolutions of orbital TIR spectra from the Mars Global Surveyor Thermal Emission Spectrometer (TES) [e.g., *Bandfield*, 2002] and recognition of mineral-specific features in VNIR spectra from telescopes [e.g., *Mustard and Sunshine*, 1995; *Bell et al.*, 1997] and orbiting spectrometers on the Phobos 2, Mars Express, and Mars Reconnaissance Orbiter spacecraft [e.g., *Bibring et al.*, 2005; *Murchie et al.*, 2007] have allowed unambiguous identifications of some minerals at global and regional scales, but the determination of complete mineral assemblages is either not possible or subject to modeling uncertainties and nonunique solutions. The recognition that weathered coatings occur commonly on Martian rocks [*McSween et al.*, 2004; *Haskin et al.*, 2005] further complicates the spectroscopic identification of primary minerals.

[3] Mineralogic interpretations of VNIR spectra measured on the Martian surface, obtained by the Viking [*Guinness et al.*, 1987], Mars Pathfinder [*McSween et al.*, 1999; *Bell et al.*, 2000], and Mars Exploration Rovers (MER) [*Bell et al.*, 2004a, 2004b] missions, have been limited by spectral resolution. These data certainly provide

[1]Department of Earth and Planetary Sciences, University of Tennessee, Knoxville, Tennessee, USA.
[2]Department of Geological Sciences, Arizona State University, Tempe, Arizona, USA.
[3]NASA Johnson Space Center, Houston, Texas, USA.
[4]Department of Physics, University of Guelph, Guelph, Ontario, Canada.
[5]Institut fur Anorganische und Analytische Chemie, Johannes Gutenberg-Universität, Mainz, Germany.
[6]National Museum of Natural History, Smithsonian Institution, Washington, D. C., USA.
[7]NASA Marshall Space Flight Center, Huntsville, Alabama, USA.
[8]Division of Geological and Planetary Sciences, California Institute of Technology, Pasadena, California, USA.
[9]Department of Astronomy, Cornell University, Ithaca, New York, USA.
[10]Jet Propulsion Laboratory, California Institute of Technology, Pasadena, California, USA.

0148-0227/08/2007JE002970$09.00

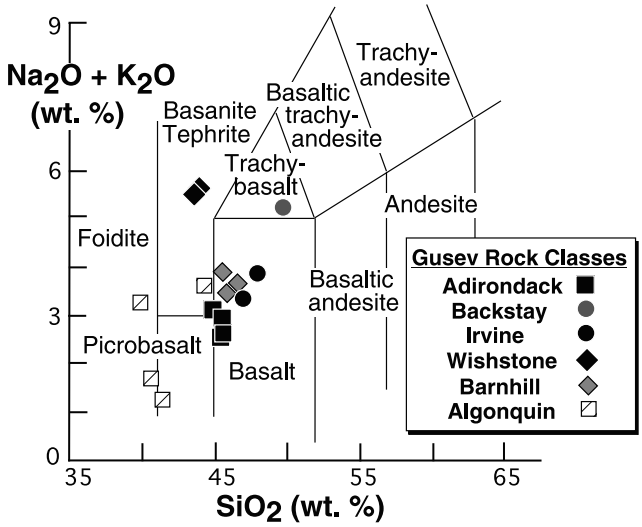

Figure 1. Petrologic classification of Gusev volcanic rocks, based on abundances of bulk alkalis versus silica (Table 1) [*Le Bas et al.*, 1986].

useful constraints, but not a full accounting of the major mineralogy of rocks. However, the MER Athena instrument package [*Squyres et al.*, 2003] includes a variety of instruments that, when used in concert, permit more detailed mineralogical assessments of Martian rocks. These instruments include Mössbauer spectrometers capable of identifying iron-bearing minerals, Alpha Particle X-ray Spectrometers (APXS) whose chemical analyses can be recast into normative mineralogy, and Miniature Thermal Infrared Spectrometers (Mini-TES) that provide diagnostic TIR spectra. Data from these instruments can be used to identify and constrain the proportions of the major phases comprising a rock's mineral assemblage.

[4] In this paper, we attempt to derive internally consistent mineral data sets for igneous rocks at the Spirit (MER) landing site in Gusev Crater. Mössbauer mineralogical data (reported previously as "areas for component subspectra" [*Morris et al.*, 2006a, also Iron mineralogy and aqueous alteration in the Columbia Hills of Gusev Crater from Husband Hill through Home Plate by the Mars Exploration Rover Mössbauer Spectrometer, manuscript in preparation, 2008]) give the percentage distribution of iron among Fe-bearing phases, but not the actual modal proportions of those phases unless the concentrations of iron in them can be independently modeled. Moreover, Mössbauer cannot detect iron-absent minerals such as feldspars and phosphates. In the present study, we recast Mössbauer subspectral areas into mineral weight percentages and correct these proportions for minerals not analyzed by Mössbauer (the latter are estimated from normative minerals calculated from APXS chemical data). Normative calculations assume equilibrium crystallization under anhydrous conditions, so this procedure is applicable only to relatively unaltered rocks. We then construct synthetic thermal emission spectra for these results and compare them with measured Mini-TES spectra for the various rock classes (see *Ruff et al.* [2006], supplemented by unpublished data, 2007) to assess whether other phases might be present. A preliminary calculation using Mössbauer data and normative mineralogy was previously used to estimate the mineralogy of several rocks at the Spirit landing site [*McSween et al.*, 2006a]. The current study expands the coverage to all relatively unaltered Gusev igneous rock classes and refines the mineral calculations using improved estimates of the iron contents of minerals, yielding slightly different results. The minimally altered igneous rock classes in Gusev Crater, defined (as are terrestrial volcanic rocks) on the basis of geochemistry [*Squyres et al.*, 2006, also Rocks of the Columbia Hills: 2: Husband Hill summit region to Home Plate, manuscript in preparation, 2008], include Adirondack, Irvine, Wishstone, Backstay, Algonquin, and Barnhill. Although only a few rock specimens of each class have been fully characterized by APXS and Mössbauer, these rock classes are reasonably abundant along Spirit's traverse through Gusev Crater and numerous samples of each class have been recognized from their distinctive Mini-TES spectra [*Ruff et al.*, 2006, also unpublished data, 2007].

[5] Unfortunately, the analytical approach applied here cannot be used to determine the mineralogy of the more pervasively altered rock classes that occur on the Columbia Hills in Gusev Crater [*Squyres et al.*, 2006, also manuscript in preparation, 2008] or of evaporitic rocks at the Opportunity rover landing site in Meridiani Planum [*Squyres and Knoll*, 2005]. The iron contents of various phases identified by Mössbauer (jarosite and an unassigned "Fe3D3" phase at Meridiani [*Morris et al.*, 2006b]) cannot be specified, and the possibility of phyllosilicates or other abundant secondary phases in altered rocks at both sites [*Clark et al.*, 2005, 2007; *Wang et al.*, 2006; *Glotch et al.*, 2006] makes calculations of meaningful normative mineralogy impossible. Other papers have already addressed the mineralogy of altered rocks at Gusev [*Ming et al.*, 2006; *Morris et al.*, 2006a; *Ruff et al.*, 2006] and Meridiani [*Clark et al.*, 2005; *Glotch et al.*, 2006; *Morris et al.*, 2006b].

2. Methods

2.1. Samples, Criteria for Selection, and Chemical Normalization

[6] For this study, rock samples generally met the following criteria:

[7] 1. Rock textures and compositions were consistent with origins as primary or mechanically reworked igneous rocks.

[8] 2. Only rocks that had been abraded (or brushed, if no abrasion was done) using the Rock Abrasion Tool (RAT) were studied. Exceptions were made for Irvine and Esperanza, for which only relatively clean, natural surfaces were analyzed.

[9] 3. Both APXS and Mössbauer analyses for the same rocks were made.

[10] 4. Rocks had experienced only limited alteration [*Morris et al.*, 2006a], as indicated by the Mössbauer-determined mineral alteration index "MAI" (defined as the sum of subspectral areas for nanophase oxide (npOx) + hematite + goethite + ferric sulfate) $\leq$ 30. Other altered rock classes in the Columbia Hills generally have MAI > 70. Even though Peace class rocks have MAI $\sim$15, they are interpreted as sandstones with abundant sulfate cement [*Squyres et al.*, 2006] and so were not included.

[11] Samples representing each rock class that met these criteria are listed below. The petrologic classifications of these rocks (Figure 1) are based on abundances of total alkalis and silica, following a commonly used classification system for volcanic rocks [*Le Bas et al.*, 1986].

Table 1. APXS Analyses and Mössbauer Subspectral Areas, Oxidation States, and Mineral Alteration Indices[a]

	Rock Class							
	Adirondack				Irvine		Wishstone	
	Adr	Hmp	Maz	Rt66	Irv	Esp	Wsh	Chm
Chemical Analyses,[b] wt %								
SiO_2	45.7	45.9	45.8	44.8	47.0	47.9	43.8	43.5
TiO_2	0.48	0.55	0.59	0.59	1.06	1.05	2.59	2.96
Al_2O_3	10.9	10.7	10.7	10.8	8.29	8.40	15.0	14.8
Fe_2O_3	3.55	3.55	2.10	1.40	7.68	9.20	5.16	6.25
Cr_2O_3	0.61	0.60	0.54	0.53	0.20	0.20	0.00	0.00
FeO	15.6	15.6	17.0	15.9	12.3	11.9	6.96	6.88
MnO	0.41	0.41	0.42	0.39	0.36	0.38	0.22	0.25
MgO	10.8	10.4	9.72	8.67	10.6	8.45	4.50	3.98
CaO	7.75	7.84	8.02	7.83	6.03	5.57	8.89	8.75
Na_2O	2.41	2.54	2.78	2.88	2.68	3.40	4.98	5.02
K_2O	0.07	0.10	0.16	0.23	0.68	0.52	0.57	0.53
P_2O_5	0.52	0.56	0.65	0.74	0.97	0.91	5.19	5.05
SO_3	1.23	1.28	1.48	4.20	2.37	2.36	2.20	1.96
Cl	0.20	0.26	0.23	0.55	0.45	0.47	0.35	0.60
Subspectral Areas, %								
A_{Ol}	47	47	57	57	10	10	20	20
A_{Px}	33	34	32	37	46	46	29	27
A_{Il}	0	0	0	0	0	0	8	7
A_{Mt}	13	11	6	0	35	35	12	9
A_{Hm}	1	2	0	0	2	2	14	11
A_{npOx}	6	7	5	7	2	2	16	12
Oxidation State and Mineral Alteration Index								
Fe^{3+}/Fe_{Total}	0.17	0.17	0.10	0.07	0.36	0.41	0.40	0.45
MAI	7	9	5	7	4	4	30	23

	Rock Class							
	Backstay	Algonquin				Barnhill		
	Bks	LaB	Sem	Alg	Com	Pos	PaS	PaC
Chemical Analyses,[c] wt %								
SiO_2	49.5	39.7	44.1	40.6	41.3	45.4	46.0	46.6
TiO_2	0.93	1.19	0.61	0.35	0.25	1.01	0.93	1.11
Al_2O_3	13.3	8.49	7.72	4.00	2.93	9.31	9.30	9.98
Fe_2O_3	3.44	4.56	5.15	2.59	5.53	8.73	9.77	8.90
Cr_2O_3	0.15	0.19	0.39	0.87	0.71	0.32	0.39	0.34
FeO	10.7	16.4	14.7	18.9	17.6	7.54	8.117.39	
MnO	0.24	0.37	0.36	0.38	0.43	0.32	0.31	0.29
MgO	8.31	11.2	12.4	22.3	24.8	9.48	9.59	10.3
CaO	6.04	6.40	4.66	2.61	1.93	6.65	6.50	6.74
Na_2O	4.15	2.78	2.98	1.59	1.12	3.50	3.25	3.36
K_2O	1.07	0.54	0.66	0.12	0.04	0.42	0.21	0.32
P_2O_5	1.39	2.89	0.91	0.63	0.45	1.37	1.12	1.27
SO_3	1.52	4.80	4.65	4.32	2.69	4.81	3.75	2.91
Cl	0.35	0.93	1.24	0.87	0.61	1.94	1.74	1.35
Subspectral Areas,[d] %								
A_{Ol}	35	72	68	73	52	18	16	16
A_{Px}	37	3	6	13	26	23	46	46
A_{Il}	3	4	0	1	0	0	0	0
A_{Mt}	11	6	5	5	2	11	32	32
A_{Hm}	2	0	0	0	4	2	0	0
A_{npOx}	13	16	20	7	17	13	27	27
Oxidation State and Mineral Alteration Index, %								
Fe^{3+}/Fe_{Total}	0.23	0.20	0.24	0.11	0.22	0.51	0.52	0.52
MAI	15	16	20	7	21	15	27	27

[12] Adirondack class basalts are Adirondack, Humphrey, Mazatzal, and Route 66. All were RAT-abraded except Route 66, which was brushed. All these basalts were encountered on the Gusev plains; although additional Adirondack class basalts were identified on Husband Hill by Mini-TES [*Ruff et al.*, 2006]; none were analyzed with other instruments.

[13] Irvine class alkali basalts are Irvine and Esperanza. Both rocks were unbrushed. Irvine occurs near the crest of Husband Hill, in an aligned group of aphanitic rocks that might be the surface expression of a dike [*McSween et al.*, 2006a]. Esperanza is a highly vesicular basalt from the Inner Basin near Home Plate; although texturally distinct, it has a similar composition to Irvine.

[14] Wishstone class tephrites (hawaiites) are Wishstone and Champagne. Both rocks were abraded. They occur as float on the northwest face of Husband Hill. Microscopic images reveal clastic textures, and *Squyres et al.* [2006] interpreted Wishstone class tephrites as possible pyroclastic rocks.

[15] Backstay class trachybasalt is Backstay. This rock was brushed. It is aphanitic and occurs as float on Husband Hill.

[16] Algonquin class picrites/foidites/basanites are from Larry's Bench, Seminole, Algonquin, and Comanche. On the basis of their very high magnesium contents, some of these rocks might actually be classified as komatiites. All these rocks were brushed. They occur as outcrops containing abundant olivine megacrysts on the southern slope of Haskin Ridge, east of Husband Hill.

[17] Barnhill class basalts are Posey and two analyses (Stars and Crawford) of Cool PapaBell. These rocks were brushed. These Barnhill class rocks are outcrops on the north side of Home Plate. *Squyres et al.* [2007] interpreted them as pyroclastic materials, possibly reworked by aeolian processes.

[18] In this paper, capitalized mineral abbreviations (e.g., Fo, En, An) refer to end-member compositions of solid solution minerals. Lowercase mineral abbreviations refer to mineral proportions calculated using the CIPW norm procedure. Normative minerals and their abbreviations are quartz (qz), corundum (cor), plagioclase (plag), orthoclase (or), albite (ab), anorthite (an), diopside (di), wollastonite (wo), enstatite (en), ferrosilite (fs), hypersthene (hy), olivine (ol), forsterite (fo), fayalite (fa), magnetite (mt), chromite (cm), hematite (hm), ilmenite (il), and apatite (ap).

Notes to Table 1.

[a]Rock name abbreviations (sol of APXS analysis) are Adr, Adirondack (A34); Hmp, Humphrey (A60); Maz, Mazatzal (A86); Rt66, Route 66 (A100); Irv, Irvine (A600); Esperanza (A1055); Wsh, Wishstone (A335); Chm, Champagne (A357); Bks, Backstay (A511); LaB, Larrys Bench (A660); Sem, Seminole Abiaka (A675); Alg, Algonquin (A688); Com, Comanche Palomino (A700); Pos, Posey (A754); PaS, Cool PapaBell Stars (A763); PaC, Cool PapaBell Crawford (A764). Mössbauer subspectral areas (for olivine, pyroxene, ilmenite, magnetite, hematite, and nanophase oxide), Fe^{3+}/Fe_{Total}, and mineral alteration index (MAI) (sum of subspectral areas for nanophase oxide + hematite + goethite + ferric sulfate) reported by *Morris et al.* [2006a].

[b]APXS analyses are from *Gellert et al.* [2006].

[c]APXS analyses from D.W. Ming et al. (manuscript in preparation, 2008).

[d]Subspectral areas for Stars and Crawford are based on one MB measurement for PaS.

Table 2a. CIPW Norms Calculated From APXS Analyses From Table 1 Corrected for SO_3 and Cl[a]

	Rock Class							
	Adirondack				Irvine		Wishstone	
	Adr	Hmp	Maz	Rt66	Irv	Esp	Wsh	Chm
qz						1.6		0.4
cor							2.4	2.1
plag	39.5	39.6	41.0	41.6	35.3	38.0	55.7	56.1
or	0.4	0.6	1.0	1.4	4.0	3.1	3.4	3.1
ab	20.4	21.5	23.7	24.4	22.7	28.8	42.1	42.5
an	18.7	17.5	16.3	15.8	8.6	6.1	10.2	10.5
di	13.5	14.7	16.1	15.2	12.2	12.7	0	0
wo	6.8	7.4	8.1	7.6	6.3	6.5		
en	3.5	3.7	3.7	3.4	3.8	3.8		
fs	3.2	3.6	4.4	4.2	2.1	2.4		
hy	16.0	15.1	7.5	6.8	32.8	27.9	13.7	13.0
en	8.3	7.7	3.4	3.0	21.0	17.2	9.7	9.9
fs	7.7	7.4	4.1	3.8	11.8	10.7	4.0	3.1
ol	21.7	21.1	27.8	25.6	1.8	0	1.5	0
fo	10.7	10.2	12.0	10.7	1.1		1.0	
fa	11.0	10.9	15.8	14.9	0.7		0.5	
mt	5.2	5.2	3.0	2.0	11.0	13.3	7.5	9.1
cm	0.9	0.9	0.8	0.8	0.3	0.3	0	0
hm	0	0	0	0	0	0	0	0
il	0.9	1.0	1.1	1.1	2.0	2.0	4.9	5.6
ap	1.2	1.3	1.5	1.8	2.3	2.2	12.3	12.0

	Rock Class							
	Backstay	Algonquin				Barnhill		
	Bks	LaB	Sem	Alg	Com	Pos	PaS	PaC_
qz							1.9	0.5
plag	55.9	35.8	34.8	17.6	12.6	40.6	38.9	41.5
or	6.3	3.2	3.9	0.7	0.2	2.5	1.2	1.9
ab	35.1	23.5	25.2	13.5	9.5	29.6	27.5	28.4
an	14.5	9.1	5.7	3.4	2.9	8.5	10.2	11.2
di	5.2	2.6	9.4	4.4	3.1	12.4	11.7	11.0
wo	2.7	1.3	4.8	2.3	1.6	6.5	6.2	5.8
en	1.5	0.7	2.7	1.4	1.0	4.8	4.5	4.4
fs	1.1	0.6	1.9	0.8	0.5	1.1	1.0	0.8
hy	11.8	9.3	14.1	13.8	26.8	22.6	23.8	25.1
en	6.7	4.9	8.2	8.8	18.5	18.4	19.3	21.2
fs	5.1	4.4	5.9	5.0	8.3	4.2	4.5	3.8
ol	16.1	31.0	25.0	52.0	44.1	0.3	0	0
fo	8.8	15.6	14.0	31.8	29.6	0.2		
fa	7.3	15.4	11.0	20.2	14.5	0.1		
mt	4.8	6.6	7.5	3.8	8.0	12.7	14.2	12.9
cm	0.2	0.3	0.6	1.3	1.1	0.5	0.6	0.5
hm	0	0	0	0	0	0	0	0
il	1.8	2.3	1.2	0.7	0.5	1.9	1.8	2.1
ap	3.3	7.1	2.2	1.5	1.1	3.2	2.7	3.0

[a]Normative mineralogy are in wt %.

[19] APXS chemical analyses for Gusev rocks were presented by *Gellert et al.* [2006] and D.W. Ming et al. (Geochemical properties of rocks and soils in Gusev Crater, Mars: Results of the Alpha-Particle X-ray Spectrometer from Cumberland Ridge to Home Plate, manuscript in preparation, 2008). Their analyses for RAT-abraded or RAT-brushed rocks are reproduced in Table 1; the reader is referred to the original references for discussion of analytical uncertainties. Some rocks had multiple analyses, and the analyses we used are identified by the sols during which APXS measurements were performed (footnote to Table 1). Mössbauer subspectral areas and MAI values [*Morris et al.*, 2006a, also manuscript in preparation, 2008] are also given in Table 1. We recast chemical data into normative mineralogy using the CIPW norm calculation procedure (available in any igneous petrology text). For norms calculations, iron was partitioned between FeO and Fe_2O_3 based on Fe^{3+}/Fe_{Total} ratios determined by Mössbauer spectroscopy (Table 1) (data from *Morris et al.* [2006a, also manuscript in preparation, 2008]). We calculated norms twice, using different procedures for removing sulfur and chlorine from APXS analyses. Some workers [e.g., *Ming et al.*, 2006] have hypothesized that sulfur and chlorine condensed onto Gusev rocks from volcanic exhalations, implying that they were unaccompanied by cations. For that model we simply subtracted SO_3 and Cl and renormalized the remaining oxides. Other workers [e.g., *King and McSween*, 2005] have suggested that sulfur and chlorine were precipitated as secondary minerals from fluids, so that they were accompanied by cations. Sulfur correlates with magnesium in Husband Hill rocks [*Ming et al.*, 2006] and

Table 2b. CIPW Norms Calculated From APXS Analyses From Table 1 Corrected for $MgSO_4$ and NaCl[a]

	Rock Class							
	Adirondack				Irvine		Wishstone	
	Adr	Hmp	Maz	Rt66	Irv	Esp	Wsh	Chm
qz					2.9	5.4	2.8	5.1
cor							2.9	3.0
plag	38.8	38.5	40.1	39.8	33.7	36.4	53.4	51.5
or	0.4	0.6	1.0	1.4	4.0	3.1	3.4	3.1
ab	18.9	19.2	22.0	20.5	19.4	25.3	39.7	37.9
an	19.5	18.7	17.1	17.9	10.3	8.0	10.3	10.5
di	12.8	13.7	15.4	13.6	10.8	11.2	0	0
wo	6.5	6.9	7.7	6.7	5.5	5.7		
en	3.2	3.4	3.4	2.6	3.2	3.2		
fs	3.2	3.5	4.3	4.3	2.0	2.3		
hy	21.5	22.4	13.4	22.7	33.0	25.6	13.1	10.5
en	10.8	11.1	5.8	8.5	20.3	14.9	8.4	7.4
fs	10.7	11.4	7.5	14.2	12.8	10.7	4.7	3.1
ol	16.7	14.9	22.3	10.5	0	0	0	0
fo	8.0	7.0	9.2	3.7				
fa	8.7	7.9	13.1	6.8				
mt	5.2	5.2	3.0	2.0	11.1	13.3	7.5	9.1
cm	0.9	0.9	0.8	0.8	0.3	0.3	0	0
hm	0	0	0	0	0	0	0	0
il	0.9	1.0	1.1	1.1	2.0	2.0	4.9	5.6
ap	1.2	1.3	1.5	1.8	2.3	2.2	12.3	12.0

	Rock Class							
	Backstay	Algonquin				Barnhill		
	Bks	LaB	Sem	Alg	Com	Pos	PaS	PaC_
qz						11.7	12.1	8.5
cor		0.2						
plag	54.7	32.2	30.6	14.5	10.4	33.8	32.8	36.9
or	6.6	3.2	3.9	0.7	0.2	2.5	1.2	1.9
ab	32.5	16.7	16.1	7.0	5.0	15.2	14.6	18.5
an	15.9	12.3	10.6	6.8	5.2	16.1	17.0	16.5
di	4.1	0	5.4	1.6	1.1	6.4	6.3	6.9
wo	2.1		2.8	0.8	0.6	3.3	3.3	3.6
en	1.1		1.4	0.5	0.4	2.3	2.4	2.7
fs	0.9		1.3	0.3	0.2	0.7	0.7	0.6
hy	20.3	33.2	42.6	34.9	40.9	19.8	21.7	23.3
en	11.1	15.5	22.6	21.3	27.8	15.2	16.8	19.2
fs	9.3	17.7	20.0	13.6	13.1	4.6	4.9	4.1
ol	8.8	10.0	1.4	33.8	32.1	0	0	0
fo	4.6	4.4	0.7	19.8	21.1			
fa	4.2	5.6	0.7	14.0	11.0			
mt	4.8	6.6	7.5	3.8	8.0	12.7	14.2	12.9
cm	0.2	0.3	0.6	1.3	1.1	0.5	0.6	0.5
hm	0	0.0	0.0	0.0	0.0	0.0	0.0	0.0
il	1.8	2.3	1.2	0.7	0.5	1.9	1.8	2.1
ap	3.3	7.1	2.2	1.5	1.1	3.2	2.7	3.0

[a]Normative mineralogy are in wt %.

no iron sulfides have been detected by Mössbauer [*Morris et al.*, 2006a], so the second model removed sulfur as $MgSO_4$ (and chlorine as NaCl). Normative mineral proportions calculated using these two chemical models are presented in Tables 2a and 2b. Comparison of these norms reveals problems with the second model (Table 2b): High proportions of hypersthene (hy) relative to olivine (ol) are inconsistent with Mössbauer and Mini-TES data, and high proportions of quartz (qz) or another silica phase in Barnhill class rocks would likely have been detected by Mini-TES. Therefore, we have utilized the normative mineral proportions in Table 2a in subsequent calculations.

2.2. Calculation Procedure

[20] For each rock, Mössbauer subspectral areas (Table 1) were converted to weight percentages of olivine, pyroxene, ilmenite, magnetite, hematite, and nanophase oxides. Previous studies [e.g., *Fegley et al.*, 1995] have converted Mössbauer subspectral areas into weight percent minerals using Debye-Waller factors (fractions of recoilless absorbed gamma rays); relative Debye-Waller factors have already been included in deriving MER Mössbauer peak areas, and previous work using these factors [*Morris et al.*, 1995] has demonstrated that the correct Fe^{3+}/Fe_{Total} ratios are obtained for rocks having varying mineralogy and oxidation states comparable to those of Gusev rocks. Our procedure for modeling the iron contents of phases and determining their weight percentages uses both Mössbauer data (Table 1) and the calculated CIPW norms (Table 2a), as described below:

[21] 1. For olivine and pyroxene, the numbers of iron atoms per formula unit (Fe_i*) were determined from mineral compositions in the CIPW norm. For olivine, Fe_{Ol}* was based on the normative Mg_2SiO_4 (fo) and Fe_2SiO_4 (fa) values. For pyroxene, Fe_{Pyx}* was based on the normative $Mg_2Si_2O_6$ (en), $Fe_2Si_2O_6$ (fs), and $Ca_2Si_2O_6$ (wo) values. Tabulated Mössbauer data do not distinguish orthopyroxene and clinopyroxene, so we summed the en, fs, and wo values in normative diopside (di) and hypersthene (hy) to model average pyroxene compositions. Fe_{Ol}* and e_{pyx}* were calculated as follows:

$$Fe_{ol}* = (fa/(fa + fo))*2,$$

where each fa formula unit contains 2 Fe + Mg atoms,

$$Fe_{pyx}* = (fs/(fs + en + wo))*2,$$

where each fs formula unit contains 2 Fe + Mg atoms.

[22] Fe_i* values for other iron-bearing phases were assigned as follows: For ilmenite $FeTiO_3$, Fe_{ilm}* = 1.0. For magnetite Fe_3O_4, Fe_{Mt}* = 2.6, assuming that the magnetite in these rocks is actually a solid solution with ulvöspinel Fe_2TiO_4. The Mössbauer spectrum for magnetite in the MIL 03346 nakhlite (a Martian meteorite) is indistinguishable from that for Spirit magnetite [*Morris et al.*, 2006c], and nakhlite magnetite contains ~40 mol % ulvöspinel on average [*Day et al.*, 2006], corresponding to Fe_{Mt}* = 2.6. If Gusev rocks had contained pure ulvöspinel rather than Ti-bearing magnetite, Mössbauer spectra could have distinguished these phases. For hematite Fe_2O_3, Fe_{Hm}* = 2, and for nanophase oxide, Fe_{npOx}* = 1.5. The latter value assumes that npOx is an equal mixture of Fe_2O_3 and FeO(OH).

[23] 2. We calculated the molecular weights (M_i) for each mineral. We assigned the following M_i values (g mol^{-1}) to ilmenite (152), magnetite (229), hematite (160) and npOx (124), on the basis of their compositions in step 1. For olivine and pyroxene, we first calculated the corresponding magnesium and calcium atoms per formula unit according to:

$$Mg_{ol}* = (fo/(fo + fa))*2$$

$$Mg_{pyx}* = (en/(en + fs + wo))*2$$

$$Ca_{pyx}* = (wo/(en + fs + wo))*2$$

We then calculated the molecular weights for olivine and pyroxene according to the formulas

$$M_{ol} = (Fe_{ol}**M_{Fa} + Mg_{ol}**M_{Fo})/2$$

where M_{Fa} is the molecular weight of fa (204) and M_{Fo} is the molecular weight of fo (141).

$$M_{px} = \left(Fe_{pyx}**M_{Fs} + Mg_{pyx}**M_{En} + Ca_{pyx}**M_{Wo}\right)/2$$

where M_{Fs} is the molecular weight of fs (264), M_{En} is the molecular weight of en (201), and M_{Wo} is the molecular weight of wo (232).

[24] 3. To calculate the weight proportion (W_i) of each iron-bearing phase, we divided the Mössbauer subspectral area for each phase (A_i, Table 1) by its Fe_i*, and then multiplied that by the corresponding molecular weight (M_i) from step 2.

$$W_i = A_i/Fe_i**M_i$$

[25] 4. We then corrected the Mössbauer-determined values W_i in step 3 by renormalizing to 100% minus the sum of the normative proportions of iron-absent minerals not measured by Mössbauer: plagioclase (plag), apatite (ap), and chromite (cm). (Note that chromite is potentially detectable by Mössbauer, but none was actually detected; it is possible that chromium is contained in olivine and pyroxene.) The rock modes (Table 3) consist of the weight percentages of iron-bearing minerals calculated in this manner, plus the normative proportions of plagioclase, apatite, and chromite (the norm also calculates minerals in weight percent, so they can be directly included).

[26] A sample calculation of mineral abundances, for the rock Adirondack, is given in Appendix A.

2.3. Calculation Uncertainties

[27] The iron contents of most phases are accurately modeled by the procedure above, but assuming an ulvöspinel content for magnetite introduces some uncertainties in calculated oxide and silicate abundances. Adding more Fe^{2+} to magnetite (in the form of ulvöspinel) makes less Fe^{2+} available for silicates, increasing the normative proportion of olivine (ol) at the expense of pyroxene (hy). Other substituting impurities (e.g., aluminum in magnetite or

Table 3. Mineral Abundances and Compositions Determined From Calculated Norms and Recalculated Mössbauer Data[a]

	Rock Class							
	Adirondack				Irvine		Wishstone	
	Adr	Hmp	Maz	Rt66	Irv	Esp	Wsh	Chm
Olivine	23.3	22.7	24.8	22.9	5.6	5.8	7.6	7.0
fo[b]	*49*	*48*	*43*	*42*	*61*	*61*	*73*	*73*
Pyroxenes[c]	30.1	30.6	29.2	31.4	46.7	44.3	17.0	19.3
Ortho-	*16.3*	*15.5*	*9.3*	*9.7*	*34.0*	*27.9*	*17.0*	*19.3*
Clino-	*13.8*	*15.1*	*19.9*	*21.7*	*12.7*	*12.7*	*0*	*0*
Plagioclase	39.5	39.6	41.0	41.6	35.3	38.0	55.7	56.1
an[b]	*47*	*44*	*40*	*38*	*24*	*16*	*18*	*19*
Ilmenite	0	0	0	0	0	0	1.9	1.4
Magnetite[d]	3.3	2.8	1.5	0	8.6	8.5	1.7	1.3
Chromite[d]	0.9	0.9	0.8	0.8	0.3	0.3	0	0
Hematite	0.2	0.5	0	0	0.4	0.4	1.8	1.1
npOxide	1.4	1.7	1.2	1.5	0.5	0.5	2.1	1.8
Apatite	1.2	1.3	1.5	1.8	2.3	2.2	12.3	12.0

	Rock Class							
	Backstay	Algonquin				Barnhill		
	Bks	LaB	Sem	Alg	Com	Pos	PaS	PaC
Olivine	12.7	45.0	47.3	58.0	44.5	9.4	8.8	7.2
fo[b]	*55*	*50*	*56*	*61*	*67*	*67*	*67*	*67*
Pyroxenes[c]	22.7	3.0	7.5	17.2	34.1	35.4	37.7	38.6
Ortho-	15.8	*2.3*	*4.5*	*13.0*	*30.6*	*22.9*	*25.3*	26.8
Clino-	6.9	*0.7*	*3.0*	*4.2*	*3.5*	*12.5*	*12.4*	*11.8*
Plagioclase	55.9	35.8	34.8	17.6	12.6	40.6	38.9	41.5
an[b]	*26*	*25*	*16*	*19*	*23*	*21*	*26*	*27*
Ilmenite	0.9	2.2	0	0.6	0	0	0	0
Magnetite[d]	1.9	1.9	1.6	1.6	0.6	6.1	5.2	4.2
Chromite[d]	0.2	0.3	0.6	1.3	1.1	0.5	0.6	0.5
Hematite	0.3	0	0	0	1.1	0	0.7	0.6
npOxide	2.1	4.8	6.0	2.2	4.9	4.8	5.4	4.4
Apatite	3.3	7.1	2.2	1.5	1.1	3.2	2.7	3.0

[a]Mineral abundances are in %. Italic values indicate normative mineral compositions.

[b]Olivine and plagioclase compositions are based on the norm (Table 2a). Olivine compositions for quartz-normative Chm assumed to be as in Wsh, for Esp as in Irv, and for Stars (PaS) and Crawford (PaC) as in Pos.

[c]Total pyroxene abundance based on Mössbauer data; relative proportions of orthopyroxene (Ortho-) and clinopyroxene (Clino-) are based on norm (Table 2a).

[d]Magnetite (containing an ulvöspinel component) and chromite are likely to be combined into a spinel phase.

pyroxene) are ignored. Likewise, assuming the relative proportions of Fe_2O_3 and FeO(OH) in nanophase oxides introduces some uncertainty in the npOx abundance. Although both npOx end-members contain only Fe^{3+}, the numbers of iron atoms per formula unit differ.

[28] To quantify these uncertainties, we calculated mineral abundances with magnetite and nanophase oxide modeled as pure phases composed of each of the end-members above for the rocks containing the highest proportions of magnetite and nanophase oxides. Consider first Irvine, for which we calculate 8.6 wt % magnetite (Table 3). An ulvöspinel content in magnetite greater than the assumed value of 40% is unlikely, because that would have been detected by Mössbauer. If we assume that magnetite in Irvine is pure Fe_3O_4, the calculated magnetite content would decrease to 7.6 wt %, with only minor (<0.5%) changes in olivine and pyroxene abundances. To quantify the effect of assumptions about the composition of nanophase oxide, we estimated mineral abundances assuming pure Fe_2O_3 and pure FeO(OH) in Seminole, for which we calculated 6.0 wt % npOx (Table 3). The pure Fe_2O_3 model reduces the nanophase oxide abundance to 4.6% with a 1.2% increase in olivine and 0.2% increase in pyroxene, whereas the pure FeO(OH) model increases nanophase oxide to 8.6% with 2.2% decrease in olivine and 0.4% decrease in pyroxene. These are all relatively minor effects, demonstrating that our assumptions about oxide compositions do not significantly affect the calculated mineral abundances.

2.4. Synthetic Mini-TES Spectra

[29] In principle, the Mini-TES spectrum measured for each rock can be deconvolved into its mineral assemblage.

Table 4. Mini-TES Observations Used to Produce Spectral Averages Shown in Figure 3

Class or Subclass	Rock ID_sol_name
Adirondack	p3148_sol041_sarah
Backstay	p3997_sol477_backstay
	p3487_sol525_nilgiri
	p3489_sol526_taj_mahal
	p3496_sol530_black_cat
	p3041_sol534_missile
	p3046_sol539_bartlett
	p3055_sol541_molly
	p3061_sol546_bastille
	p3073_sol554_dauphine
Irvine	p3133_sol590_irvine
	p3141_sol599_compagnoni
	p3142_sol599_unsoeld
	p3143_sol599_whillans
	p3156_sol604_adze
Wishstone	p3811_sol335_wishbone
	p3820_sol341_labrea
	p3819_sol341_golden_rings
	p3830_sol344_pipers_piping
	p3246_sol657_goldenrod
Larry's Bench	p3250_sol659_bluestem
	p3257_sol662_toadflax
	p3258_sol662_zizia
Seminole	p3269_sol668_seneca
	p3270_sol668_peoria
	p3271_sol668_seminole
	p3281_sol672_muscogee
	p3282_sol672_miccosukee
	p3283_sol672_apalachicola
	p3284_sol672_chattahoochee
	p3287_sol673_yeehaw
	p3288_sol673_palatka
Algonquin	p3272_sol668_miami
	p3298_sol682_kekionga
	p3299_sol682_meentwioni
	p3300_sol682_myaamia
	p3301_sol682_algonquin
	p3304_sol687_winneway
	p3306_sol687_barriere_lake
	p3307_sol687_eagle_village
	p3313_sol689_golden_lake
	p3314_sol689_wolf_lake
Comanche	p3324_sol695_ditsakana
	p3326_sol695_kewatsana
	p3330_sol696_tenawa
	p3333_sol698_taabe
	p3340_sol701_saupitty
Home Plate	p3474_sol747_stearnes
	p3475_sol747_mackey
	p3388_sol758_wilmington

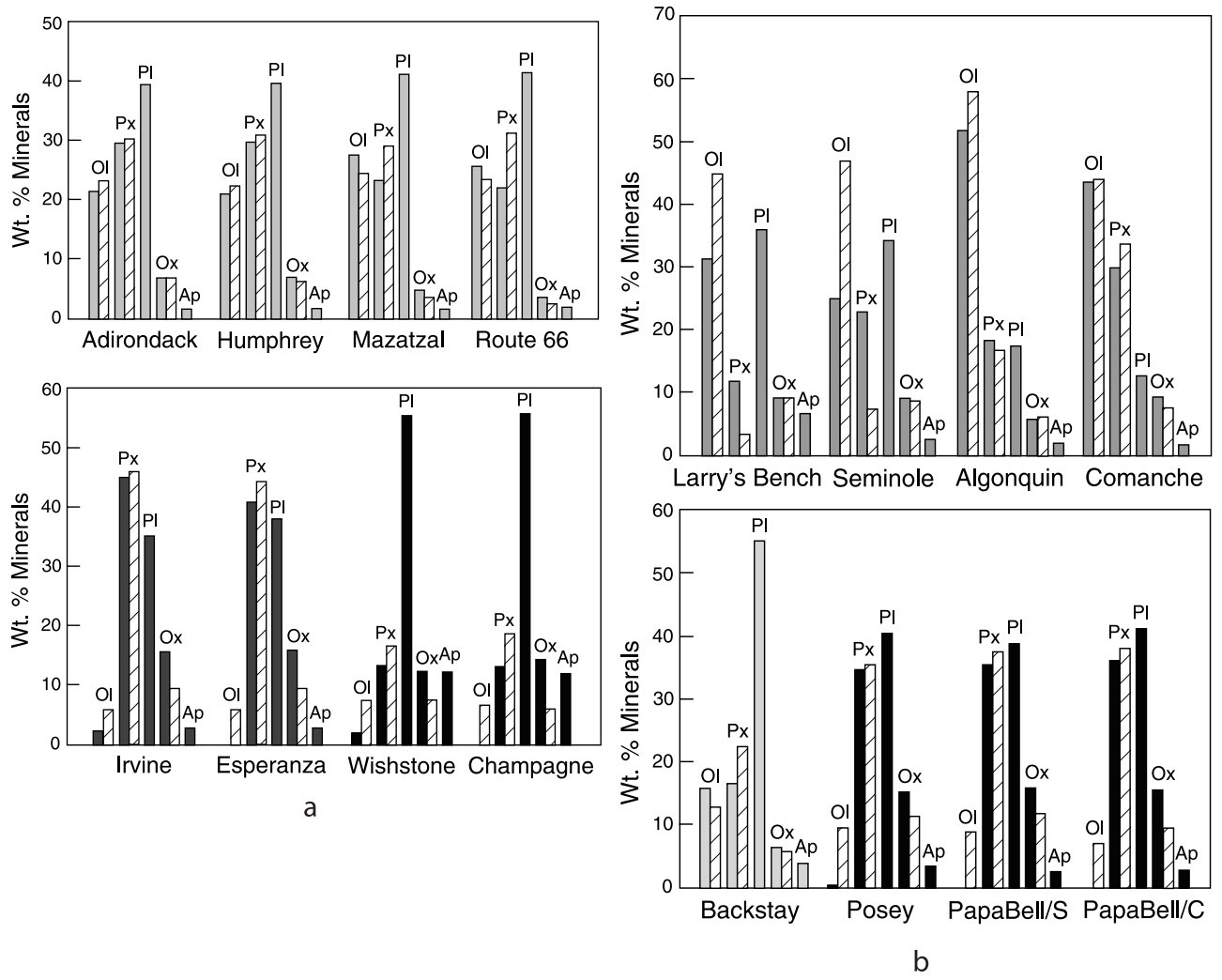

Figure 2. Comparison of the calculated normative mineral abundances (shaded bars, Table 2a) for Gusev rocks with Mössbauer-determined mineral abundances (cross-hatched bars, renormalized to take into account iron-absent minerals not detected by Mössbauer, Table 3). (a) (top) Adirondack class rocks (Adirondack, Humphrey, Mazatzal, and Route 66), and (bottom) Irvine class (Irvine and Esperanza) and Wishstone class rocks (Wishstone and Champagne). (b) (top) Algonquin class rocks (Larry's Bench, Seminole, Algonquin, Comanche), and (bottom) Backstay and Barnhill class rocks (Posey, Cool Papa Bell Stars, Cool Papa Bell Crawford).

However, spectra for most of the rocks in this study are affected by dust contamination of the Mini-TES pointing mirror, which impacts all spectra measured after sol 420 [*Ruff et al.*, 2006]. A provisional correction was developed by *Ruff et al.* [2006], but this source of uncertainty and other environmental effects on TIR spectra must be considered. Here we adopt an alternative strategy that involves calculating synthetic emissivity spectra using the mineral modes derived from APXS and Mössbauer data for direct comparison to Mini-TES spectra, as previously demonstrated by *McSween et al.* [2006a] and *Ruff et al.* [2006]. In this approach, laboratory spectra representing these mineral modes are combined in the appropriate fractional abundances to produce a synthetic spectrum for a given rock. Because the long-wavelength portions of Mini-TES spectra (<600 cm^{-1}) are least impacted by mirror dust and environmental effects [*Ruff et al.*, 2006], they provide the best opportunity for robust comparisons between measured and synthetic spectra.

[30] Olivine and plagioclase modes from APXS and Mössbauer data can be converted directly into their spectral equivalents using the normative compositional information (fo and anorthite (an), respectively). The same is not true of the pyroxene phases. Here we used an averaged spectrum of four augites to produce a "clinopyroxene" spectrum and four bronzites to produce an "orthopyroxene" spectrum, with the intent of best representing intermediate compositions rather than the solid solution end-members. Magnetite, ilmenite, and apatite normative phases have end-member spectra in the library. A chromite spectrum was not available for this work, but given the low abundance of this phase in the norms ($\leq$1.3%), its omission has little impact on the final results. The spectral character of the npOx phase obtained from Mössbauer data is uncertain, and here it has

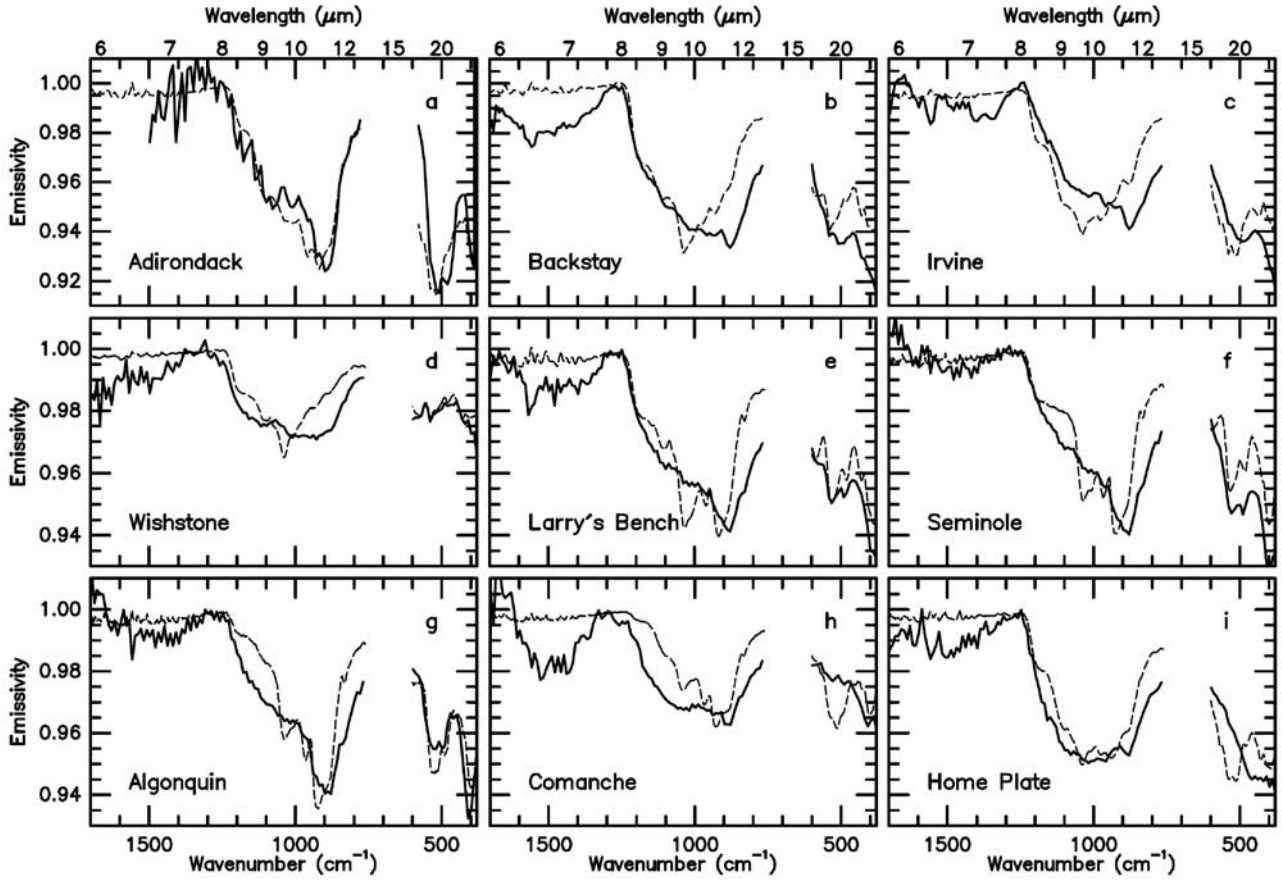

Figure 3. Comparisons of synthetic thermal emission spectra (dashed lines) based on the mineralogies of Gusev rocks (Table 3) with measured Mini-TES spectra for various rock classes (solid lines, data sources in Table 4). Home Plate rocks in Figure 3i are compared to Posey.

been represented by the spectrum of basaltic glass. The definition of npOx by *Morris et al.* [2006a] emphasizes its poorly crystalline nature that, according to *Ruff et al.* [2006], may be broadly similar to basaltic glass when measured at thermal infrared wavelengths.

[31] The measured Mini-TES spectra for the various rock classes that we used for comparison are actually averages of multiple, high-quality spectra, rather than spectra of individual rocks. The rock names, sols in which the spectra were taken, and sequence identification numbers are given in Table 4.

3. Mineral Abundances

[32] The mineral abundances for Gusev rocks estimated from Mössbauer and APXS data are presented in Table 3. These data are compared with normative mineral abundances (also in weight percent) in Figure 2.

3.1. Adirondack Class Basalt

[33] The olivine abundances for four Adirondack class basalts (Table 3) agree with the point-counted volumetric proportion (~20%) of dark crystals (thought to be olivine phenocrysts) observed in Microscopic Imager images of RAT-abraded portions of Humphrey [*McSween et al.*, 2006b]. The abundances of olivine, pyroxene, and plagioclase in Adirondack, Humphrey, Mazatzal, and Route 66 are remarkably uniform. However, Mazatzal and Route 66 have higher ratios of clinopyroxene to orthopyroxene, and their plagioclase has lower anorthite content [An#s = Ca/(Ca + Na + K) * 100]—in other words, more calcium silicate and less calcium-aluminum silicate. Mazatzal and Route 66 have nearly identical CaO and Al_2O_3 contents but higher Na_2O contents than Adirondack and Humphrey, so this difference in normative pyroxene results from the calculation of more sodic plagioclase. These two rocks also have slightly lower magnetite contents than Adirondack and Humphrey, reflecting their lower Fe^{3+}/Fe_{Total} ratios (Table 1). These apparent differences in mineral composition may be artifacts of alteration. Mazatzal and Route 66 are light-toned rocks with coatings hypothesized to have formed by interaction with aqueous fluids [*Haskin et al.*, 2005]. APXS analyses measure only the outer few micrometers of material, whereas Mössbauer analyses penetrate more deeply into the rock. Although Mazatzal was RAT-abraded, some remaining rind was seen in the Microscopic Imager (MI) image [see *McSween et al.*, 2006b, Figure 3], and Route 66 was only brushed. The apparent mineralogic differences reflect the fact that the light-toned rinds are slightly elevated in sodium and ferric iron.

3.2. Irvine Class Alkali Basalt

[34] Irvine and Esperanza have high proportions of pyroxene and magnetite, as seen in both Mössbauer and normative data, and the Mössbauer-determined and normative olivine

proportions are in fairly good agreement (Figure 2a). Despite the marked textural differences between these rocks (Irvine is aphanitic and featureless, Esperanza is vesicular), they have similar composition and mineralogy.

3.3. Wishstone Class Tephrite (Tuff?)

[35] Both rocks have especially high proportions of normative plagioclase, ilmenite, and apatite (Table 3), reflecting their very high Al_2O_3, TiO_2, and P_2O_5 contents. The plagioclase compositions are very sodic. The agreement between Mössbauer-determined and normative olivine (Figure 2a) is not very good, and Champagne actually contains a small amount of normative quartz rather than olivine (the normative olivine composition of Wishstone was used to calculate the Mössbauer olivine abundance for Champagne). The cause of this discrepancy is unknown.

3.4. Backstay Class Trachybasalt

[36] In Backstay, the Mössbauer-determined abundance of pyroxene is slightly higher than normative pyroxene, and olivine shows the opposite relationship (Figure 2b). Backstay was only RAT-brushed, so this difference may reflect a surface alteration effect. Feldspar in this rock is especially abundant, reflecting its high Al_2O_3 content, and it has high albite (ab) and orthoclase (or) normative components (Table 2a). The detection of ilmenite by Mössbauer is consistent with its high APXS-measured TiO_2 content and normative il.

3.5. Algonquin Class Picrite/Foidite/Basanite

[37] Rocks of the Algonquin class are dominated by olivine. The derived mineralogy for three of the four analyzed rocks (Larry's Bench, Seminole, and Algonquin) shows markedly higher olivine and lower pyroxene abundances, relative to normative olivine and pyroxene (Figure 2b). Of all the rocks in this study, these Algonquin class rocks show the greatest difference between Mössbauer-determined and normative mineralogy. In contrast, the Mössbauer-determined and normative abundances for olivine and pyroxene in Comanche (also classified chemically as Algonquin class) agree very well.

3.6. Barnhill Class Basalt (Tuff?)

[38] Mössbauer-determined olivine abundances for the rocks comprising Home Plate are higher than normative values (Figure 2b). The Posey norm has only a tiny amount of olivine and Cool Papa Bell analyses are slightly quartz-normative (Table 2a). This difference is in the same sense as in Algonquin rocks, but Home Plate pyroxene contents determined by the two methods agree very well. The oxide abundances show the greatest difference for any Gusev rocks (Figure 2b). The normative magnetite contents are exceptionally high (Table 2a), consistent with the high Fe^{3+}/Fe_{Total} ratios of these rocks, whereas Mössbauer data partition ferric iron between magnetite and npOx (Table 3).

4. Comparison With Thermal Emission Spectra

[39] Figure 3 shows the synthetic spectra of nine modeled rocks representing the Gusev rock classes. Humphrey's synthetic spectrum was used to represent the Adirondack class (Figure 3a) and is compared to a Mini-TES spectrum of the rock Sarah that also is representative of the class. As shown by *Ruff et al.* [2006], there is a favorable match between the synthetic and measured versions. Among all the rocks investigated here, Adirondack class basalts show the best match between the synthetic and measured spectra. This is partly a function of the fact that the spectral effects of surface dust, slope due to temperature determination error, and downwelling sky radiance were modeled and removed via deconvolution. Adirondack is one of only two rock classes in this study measured before the sol 420 mirror-dusting event and whose spectra were deconvolved and normalized to exclude these effects.

[40] Spectra for the rocks Backstay and Irvine were presented previously [*McSween et al.*, 2006a], but here we use an average of nine measured Backstay class and four Irvine class spectra [*Ruff et al.*, 2006] along with revised norms in the synthetic spectra (Figures 3b and 3c). There is no appreciable improvement in the fits, which display clear mismatches throughout most of the spectral range and are among the worst in the full set. A possible role for pigeonite [*Squyres et al.*, 2006] and/or glass [*McSween et al.*, 2006a] initially was suggested to explain the misfit. We have now ascertained that the composition of the plagioclase component also has a significant impact on the shape of the synthetic spectra, most notably in the middle wave number range ($\sim$800–1200 cm^{-1}). The modeled sodic plagioclase component (oligoclase, An_{29}) is mostly responsible for the prominent V-shaped emissivity minimum at $\sim$1050 cm^{-1} in the synthetic spectra (Figures 3b and 3c). The minimum is diminished or absent when andesine or other more calcic plagioclase spectra are substituted. Ternary (Na-K-Ca) feldspar compositions may occur in these volcanic rocks, although they are not represented in the spectral library. An alternative explanation is that the plagioclase in the rock could be a disordered form due to rapid crystallization. In this case, the measured spectra may not be well modeled by the synthetic spectra that were produced using an ordered plagioclase (oligoclase; no disordered equivalent was available).

[41] The Wishstone class (Figure 3d shows an average for four rocks) has a premirror-dusting spectrum that was deconvolved into modal mineralogy by *Ruff et al.* [2006]. The spectrally derived abundance of its plagioclase component at 55% is well matched to the normative abundance of 56.7%. However, the composition of plagioclase is quite different: An_{64} (bytownite) from spectral deconvolution versus An_{18} (oligoclase) from the norm calculation. The quality of the fit between the synthetic and measured spectra is poor in the middle wave number range and good at low wave numbers (Figure 3d). Again there is a prominent V-shaped emissivity minimum at $\sim$1050 cm^{-1} in the synthetic spectrum that produces a poor fit to the measured spectrum and is due mostly to the modeled plagioclase component. This portion of the spectrum is sensitive to plagioclase composition whereas the low wave number range is less so. Other components that affect the middle spectral range more than the low range are phosphates and sulfates. The Wishstone class is notable for its very high phosphorus content [e.g., *Ming et al.*, 2006], which here is modeled with a normative apatite abundance of 12.5%, the highest in this study. The spectrally derived phosphate phase is wavellite at $\sim$10% [*Ruff et al.*, 2006]. Although these abundances are comparable, the composition and origin of these two phosphates

are significantly different, as apatite is a common igneous accessory mineral and wavellite is a hydrous secondary mineral. *Ruff et al.* [2006] expressed uncertainty in the wavellite identification, but it is clear that apatite distorts the spectral fit to such an extent that it is an unlikely component of the rock. A sulfate component at ~10% abundance was modeled in the deconvolution of the Wishstone class spectrum [*Ruff et al.*, 2006], but sulfur is excluded from norm modeling. Most rocks in this study have measured sulfur contents well above those expected for magmatic rocks. In the case of the Wishstone class, the absence of a sulfate component in the synthetic spectrum contributes to the poor fit in the middle wave number range.

[42] The four Algonquin class rocks are notable for their high normative and Mössbauer-derived olivine abundances (>45%), twice that of Adirondack class basalts. The Mini-TES spectra of each of the named members divide into spectrally separable groups for which there were four measured Larry's Bench examples, nine Seminole examples, ten Algonquin examples, and five Comanche examples. Each group was averaged together to produce the measured spectra presented (Figures 3e, 3f, 3g, and 3h). With the exception of Comanche, these spectra clearly display prominent features readily attributable to the dominant olivine component. The synthetic spectra for Larry's Bench, Seminole, and Algonquin reflect the contributions of olivine in shaping the spectra, most notably the double-peaked emissivity feature in the low wave number region (<600 cm^{-1}) and the pronounced asymmetry of the middle wave number region with its emissivity minimum near 900 cm^{-1}. The sodic plagioclase-related feature at ~1050 cm^{-1} of the synthetic spectra diminishes the quality of the fit to the measured spectra most notably for Larry's Bench, with decreasing impact on the Seminole and Algonquin spectra that reflects its decreasing normative abundance (Table 2a) in the latter rocks. The APXS-measured SO_3 contents of these rocks approach 5%, likely due to alteration. The absence of a sulfate phase in the synthetic spectra that likely is present on the rocks could explain the poor fit to the measured spectra in the ~1100–1200 cm^{-1} range, most evident in the Algonquin spectrum (Figure 3g).

[43] Comanche has been grouped within the Algonquin class based on its chemistry, but its Mini-TES spectrum is notably different from the other three Algonquin examples (Figure 3h). It lacks any obvious olivine features in the low wave number range and displays a more symmetric absorption in the middle range. Its synthetic spectrum (reflecting the high Mössbauer-determined abundance of olivine) produces the poorest fit of any of the rocks in this study, supplying no comparable features throughout any of the spectral range. We made an initial effort to deconvolve this spectrum, but this failed to produce any indication of what phases could produce such an unusual spectrum. At this point, the spectral character of Comanche remains enigmatic.

[44] Although three examples of Barnhill rocks are considered in this study, none was a favorable target for Mini-TES observations because of surface dust and/or small size. Instead, Mini-TES observed three minimally dusty rocks at Home Plate that were spectrally indistinguishable. Their spectra have been averaged together for comparison to a synthetic spectrum for Posey (Figure 3i). The measured and synthetic spectra are broadly similar in the middle wave number range, each with a generally U-shaped and symmetrical absorption. However, there is a significant mismatch in the low wave number range. Where the synthetic spectrum displays a deep emissivity minimum near 500 cm^{-1} followed by a prominent emissivity peak at ~450 cm^{-1}, the measured spectrum has a single apparent minimum around 450 cm^{-1}. Such a feature is unique among all of the measured spectra in this study, but was a noted attribute of the altered Clovis and Watchtower class rocks encountered earlier in the mission [*Ruff et al.*, 2006]. The generally U-shaped and symmetrical absorption in the middle wave number range is common to these rocks. Spectral deconvolution of Barnhill rocks was successful (S.W. Squyres et al., also manuscript in preparation, 2008) and revealed a major basaltic glass component (~45%) that was mostly responsible for producing these spectral characteristics. Abundant glass is consistent with the pyroclastic origin of Home Plate that is favored by *Squyres et al.* [2007]. The npOx determined by Mössbauer may be spectrally equivalent to glass, if the glass contains sufficient Fe^{3+}, so it is unclear whether this oxidized component is actually npOx, glass, or a mixture of both. The relatively high magnetite contents of Barnhill class rocks determined by Mössbauer (Table 3) are not evident in the Mini-TES deconvolution, because the two strongest spectral features are mostly truncated by the exclusion range of atmospheric CO_2 and the 380 cm^{-1} limit used in the deconvolution. It would be difficult to detect the presence of magnetite at 5% abundance.

[45] The comparison of synthetic and measured Mini-TES spectra serves to highlight phases that likely are present in the rocks and those that likely are not. Olivine in its Mössbauer-derived abundance appears to be in agreement with observation in the case of Adirondack and Algonquin rocks, with the exception of Comanche. Aside from misfits that can be attributed to unmodeled sulfate and glass components, the greatest discrepancies between synthetic and measured spectra appear to be related to sodic plagioclase. It is noteworthy that the most calcic normative plagioclase occurs in Adirondack Class rocks (Table 2b) and their measured and synthetic spectra have the best fit. Wherever normative plagioclase is both abundant (>30%) and sodic (an < 40), a poor match occurs. Backstay and Irvine are the best examples of this problem. More sodic plagioclase may occur if pigeonite (which contains more calcium than orthopyroxene) is present. Pigeonite is not calculated in the norm, but might be expected in more highly fractionated volcanic rocks.

5. Mineral Compositions

[46] The normative compositions of pyroxenes, olivines, and feldspars in the various Gusev rock classes are illustrated in Figure 4, with coexisting mafic mineral compositions connected by tie lines in Figure 4 (top). Pyroxenes span a wide range of Mg/Fe ratios, with Barnhill class rocks having the most magnesian compositions (reflecting their high Fe^{3+}/Fe_{Total} ratios) and Adirondack class rocks the most ferroan compositions. Note that the plotted calcium concentrations (wo) of normative pyroxenes have no significance, as the norm always calculates pyroxenes with either 50 mol % Ca (di) or 0% Ca (hy). Olivine Mg/Fe ratios, expressed as Fo and Fa end-members (Figure 4),

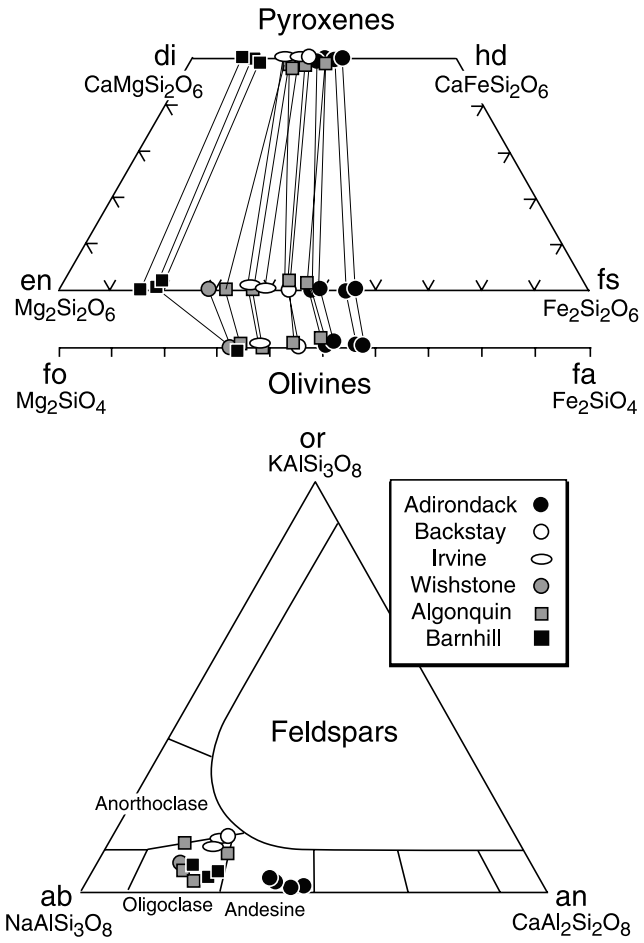

Figure 4. Normative mineral compositions in Gusev rocks. Coexisting pyroxene and olivine compositions are connected by tie lines. Mineral end-member abbreviations are diopside (di), hedenbergite (hd), enstatite (en), ferrosilite (fs), forsterite (fo), fayalite (fa), orthoclase (or), albite (ab), and anorthite (an).

show a corresponding range to pyroxenes, reflecting the fact that the norm calculates olivine compositions that are in equilibrium with pyroxenes. Normative feldspar compositions for these rocks generally plot in the fields of andesine and oligoclase, although several rocks have potassium-rich feldspars that fall on the boundary with anorthoclase (Figure 4). The various rock classes show systematic differences in feldspar composition. The normative mineral compositions should be considered as average mineral compositions, rather than the actual mineral compositions in the rocks. Volcanic rocks typically contain chemically zoned minerals formed over a range of temperatures, a phenomenon not accommodated in the norm calculation.

[47] Particularly interesting are the normative olivine compositions in Algonquin class rocks, which vary systematically with elevation (Figure 5). These data were obtained as Spirit drove down the southeast face of Husband Hill, potentially sampling lower stratigraphic levels of a common unit. Olivine abundance also increases downward (Figure 5), except for Comanche. The Mössbauer spectral component attributed to pyroxene is also distinctive in Comanche compared to other rocks in Gusev Crater (R.V. Morris et al., manuscript in preparation, 2008). This high modal abundance of olivine, plus the regular variation in olivine composition with more magnesian olivine at lower stratigraphic levels, may suggests that Algonquin lavas or a sill accumulated olivine crystals during progressive fractional crystallization.

[48] The normative mineral compositions are broadly consistent with constraints from other data sets. Similarities of Mössbauer spectral parameters to those from minerals with known compositions [*Morris et al.*, 2006a] suggest that the pyroxenes in Gusev rocks are pigeonite, augite, and orthopyroxene, but not diopside, and that olivines have compositions of $Fo_{>50}$.

[49] Mini-TES spectra can also provide constraints on the compositions of some minerals, especially olivine. In a recent study using laboratory thermal emission spectra of a suite of olivine samples ranging from Fo_1 to Fo_{93}, *Lineberger et al.* [2006] demonstrated that the exact wave number positions of three key olivine spectral features in the 550–350 cm^{-1} range exhibit strong linear correlations with composition. The sensitivities of these correlations are such that at Mini-TES spectral resolution (10 cm^{-1}), a laboratory-quality emissivity spectrum of a pure olivine sample can be used to determine its Fo value to within $\Delta Fo = 15$. Forward modeling of linear mixtures of spectral components commonly present in Spirit's Mini-TES spectra suggests that the positions of key olivine features are not shifted by these other components. Thus, we can gain some idea of olivine compositions by simply measuring the wave number positions of these features, without spectral deconvolution. Table 5 gives the Fo values for olivine in various rock classes that have significant olivine spectral features. Each class has up to three olivine compositions listed, based on the wave number positions of three spectral features (a local

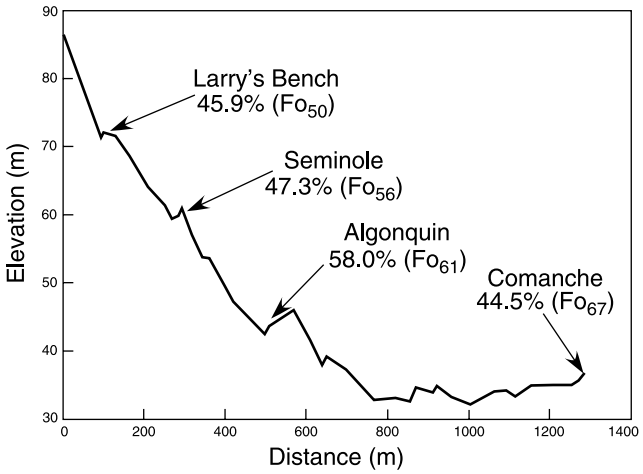

Figure 5. Spirit vertical traverse (OSU bundle-adjusted [*Li et al.*, 2006]) for sols 654 (top left) to 754 (lower right) on the southwest side of Husband Hill. The positions of Algonquin class rocks and their olivine modal abundances (wt %) and compositions (Fo) are shown. These mineralogic variations may result from olivine accumulation at various stratigraphic levels that were encountered as the rover drove downhill. (Adapted from *Li et al.* [2006].)

Table 5. Olivine Compositions Inferred From Mini-TES Spectral Features[a]

	Feature		
Rock Class	500 cm^{-1}	450 cm^{-1}	400 cm^{-1}
Adirondack	Fo49	Fo56	
Backstay	Fo49	Fo87	
Irvine		Fo72	
Algonquin	Fo84	Fo72	Fo58

[a]Olivine compositions are in mol % Fo.

minimum near ~500 cm^{-1}, a local maximum near ~450 cm^{-1}, and a local minimum near ~400 cm^{-1}). To improve signal-to-noise, averaged spectra created from several targets in each class were used to find the olivine features. In cases where olivine spectral features were difficult to discern, the corresponding entries are blank. In laboratory spectra, the three Fo values agree. Clearly there is some variation in the Fo values inferred from different spectral features in these Mini-TES spectra, but these data may provide some limits on olivine compositions that appear to be in broad agreement with olivine compositions estimated from norm calculations and Mössbauer data (c.f. Table 3).

6. Mineral Abundances and Alteration

[50] Adirondack and Humphrey (RAT-abraded Adirondack class basalts) show remarkable consistency among mineral abundances estimated from Mössbauer, norm, and Mini-TES data. Mazatzal (RAT-abraded, but still retaining some alteration rind) and Route 66 (RAT-brushed) show greater variations, with slightly lower olivine and higher pyroxene abundances in Mössbauer estimates (Figure 2a). Backstay (RAT-brushed) shows fairly good agreement between Mössbauer and normative olivine and pyroxene (Figure 2b). The remaining rock classes have more pronounced deviations, with higher olivine and usually lower pyroxene abundances in Mössbauer determinations relative to norms (Figure 6). In part this is due to the fact that the RAT grinding heads wore away on sol 416 after 15 uses, meaning that most of the later measurements were made on unabraded rocks. RAT-abraded Wishstone rocks show similar deviations, however.

[51] These deviations can be understood in terms of differences in the depths of rock sampled by APXS (the outer few tens of micrometers) and Mössbauer (a few hundreds of micrometers) analyses. APXS actually measures different elements to different depths within the sample (increasing with element atomic weight), which might be important if the rocks are not homogeneous. The field of view for APXS is also larger than for Mössbauer, which might relatively bias Mössbauer analyses of rocks containing heterogeneously distributed phenocrysts. Basaltic rock surfaces attacked by acidic fluids show selective dissolution of olivine [*Tosca et al.*, 2004; *Hurowitz et al.*, 2006], so it is not surprising that norms calculated from APXS analyses of unabraded rocks have somewhat lower olivine contents. It is also possible that incompletely removed dust coatings might affect olivine measurements. Figure 6 shows that there is no discernable relation between the composition of olivine (normative fo values are given) and its depletion.

[52] The indications of alteration on rock surfaces, apparently dominated by dissolution of olivine (Figure 6), suggest that measurements of natural rock exteriors will not generally provide accurate assessments of mineralogy [*Hurowitz et al.*, 2006]. Norms calculated from APXS analyses appear to be accurate reflections of the mineral assemblages in RAT-abraded rocks, but not for brushed or natural rock surfaces. Mathematical projection from the brushed composition through the abraded composition has been previously employed to estimate the chemical compositions of Adirondack class rocks [*McSween et al.*, 2006b], but projections using only brushed and natural compositions (when no abraded compositions are available) will likely give unreliable interior compositions. Because Mössbauer spectra sample the mineralogy of the deeper parts of the rock, this technique provides the most accurate measure of mineralogy, although only for iron-bearing minerals. The widespread occurrence of alteration coatings on Mars rocks may limit the usefulness of spacecraft remote sensing measurements to determine rock mineralogy.

7. Summary

[53] Determination of the complete mineral assemblages of Mars rocks is arguably among the most difficult measurements by remote sensing. Incomplete mineral inventories, as typically provided by spectroscopy, are useful but allow only partial (sometimes even potentially misleading) constraints on petrogenesis. We acknowledge that the mineral assemblages of individual rocks on Mars may have only limited utility as groundtruth for orbital measurements, because rocks rarely provide broad spatial coverage of surfaces. Nevertheless, these mineralogies provide insights into what is not being identified from orbiting spacecraft, as well as information on the conditions under which rocks formed.

[54] The Athena instrument package on the Spirit rover has provided a unique opportunity to determine the complete

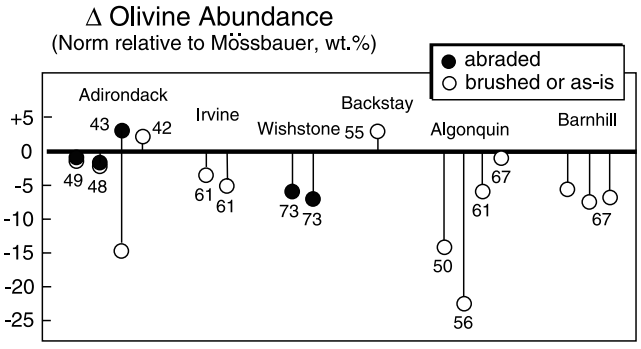

Figure 6. Differences (wt %) between the abundance of olivine measured by Mössbauer (represented by the horizontal line) and calculated normative olivine abundance (represented by dots). The better agreement for relatively unaltered rocks (Adirondack, Backstay, and Irvine classes) and for RAT-abraded rocks (solid symbols) suggests dissolution of olivine by acidic weathering at rock surfaces [*Hurowitz et al.*, 2006]. The degree of olivine depletion does not show any apparent relationship to the composition of olivine (normative fo contents are indicated).

modal mineralogies of igneous rocks in Gusev Crater. Using analyses of mostly RAT-abraded or brushed rocks, we show that Mössbauer spectra provide the most accurate assessment of abundances, but obviously only for iron-bearing minerals. We have modeled the iron contents of these minerals, using constraints from APXS normative mineralogy, and converted Mössbauer-determined subspectral areas into mineral weight percentages. These were then renormalized to 100% minus the proportions of normative minerals not detected by Mössbauer spectra (plagioclase, apatite, and chromite) to estimate the complete modal mineralogy. The abundances of iron-bearing minerals modeled from Mössbauer data agree fairly well with normative calculations, although there are some systematic differences. We also calculated synthetic thermal emission spectra for these mineral assemblages and compared them with measured Mini-TES spectra for the respective rock classes. With the exception of the Adirondack class rocks, for which agreement is excellent, the synthetic spectra do not provide particularly good fits for Mini-TES spectra. This apparently results from an inability to model the spectra of sodic plagioclase, as well as unmodeled sulfate, glass, or pigeonite components. However, olivine compositions can be estimated from Mini-TES spectral features without spectral deconvolution, and these are in broad agreement with compositions derived from other data.

[55] Differences in the penetration depths for analysis using Mössbauer and APXS spectra, coupled with the recognition that the surfaces of Gusev rocks have been altered by dissolution of olivine, can explain the modest differences in mineral abundances determined by Mössbauer and calculated from norms. The apparently widespread occurrence of mineralogically altered rock surfaces on Mars has profound implications for spacecraft remote sensing, requiring techniques that access rock interiors and further emphasizing the importance of determining complete mineral assemblages.

Appendix A: Sample Calculation for Adirondack

[56] 1. Determine the number of Fe atoms per formula unit (Fe_i') for olivine (ol) and pyroxene (px) from the CIPW norm: Fo = 10.7, Fa = 11.0, En = 11.8, Fs = 10.9, Wo = 6.8.

$$Fe_{ol}' = (Fa/(Fa + Fo))*2 = 1.01$$

$$Fe_{px}' = (Fs/(Fs + En + Wo))*2 = 0.74$$

[57] 2. Determine molecular weights (M_i) for each Fe-bearing mineral:

$$Mg_{ol}' = (Fo/(Fa + Fo))*2 = 0.99$$

$$Ca_{px}' = (Wo/(Fs + En + Wo))*2 = 0.46$$

$$Mg_{px}' = (En/(Fs + En + Wo))*2 = 0.80$$

$$M_{ol} = (Fe_{ol}'*M_{Fa} + Mg_{ol}'*M_{Fo})/2 = 172.9$$

where $M_{Fa} = 204$, $M_{Fo} = 141$

$$M_{px} = (Fe_{px}'*M_{Fs} + Mg_{px}'*M_{En} + Ca_{px}'*M_{Wo})/2 = 231.4$$

where $M_{Fs} = 264$, $M_{En} = 201$, $M_{Wo} = 232$

$$M_{ilm}(\text{ilmenite}) = 152$$

$$M_{mt}(\text{magnetite}) = 229$$

$$M_{npOx}(\text{nanophase oxide}) = 124$$

$$M_{hm}(\text{hematite}) = 160$$

[58] 3. Divide Mössbauer subspectral areas (A_i) by the number of Fe atoms per formula unit (Fe_i'):

$$A_{ol}/Fe_{ol}' = 47/1.01 = 46.53$$

$$A_{px}/Fe_{px}' = 33/0.74 = 44.59$$

$$A_{ilm}/Fe_{ilm}' = 0/1 = 0$$

$$A_{mt}/Fe_{mt}' = 13/2.60 = 5$$

$$A_{npOx}/Fe_{npOx}' = 6/1.50 = 37.33$$

$$A_{hm}/Fe_{hm}' = 1/2 = 0.5$$

[59] 4. Calculate the molecular weight of each phase that contains some proportion of Fe:

$$S_{ol} = A_{ol}/Fe_{ol}'*M_{ol} = 8,017$$

$$S_{px} = A_{px}/Fe_{px}'*M_{px} = 10,334$$

$$S_{ilm} = A_{ilm}/Fe_{ilm}'*M_{ilm} = 0$$

$$S_{mt} = A_{mt}/Fe_{mt}'*M_{mt} = 1,145$$

$$S_{hm} = A_{hm}/Fe_{hm}'*M_{hm} = 80$$

$$S_{npOx} = A_{npOx}/Fe_{npOx}'*M_{npOx} = 496$$

$$S_{total} = S_{ol} + S_{px} + S_{ilm} + S_{mt} + S_{hm} + S_{npOx} = 20,072$$

[60] 5. Renormalize to 100 wt % (W_i) minus the CIPW normative proportions (W_i) of Fe-absent minerals not measured by Mössbauer:

$$\text{plagioclase, } W_{plag} = 39.5$$

$$\text{apatite, } W_{ap} = 1.2$$

$$\text{chromite, } W_{crm} = 0.9$$

$$W_{\text{nonFe minerals}} = W_{plag} + W_{ap} + W_{crm} = 41.6$$

$$W_{\text{Fe minerals}} = W_{ol} + W_{px} + W_{ilm} + W_{mt} + W_{hm} + W_{npOx} = 58.4$$

$$\text{olivine, } W_{ol} = S_{ol}/(S_{total}*W_{\text{Fe minerals}}) = 23.3$$

$$\text{pyroxene, } W_{px} = S_{px}/(S_{total}*W_{\text{Fe minerals}}) = 30.1$$

$$\text{ilmenite, } W_{ilm} = S_{ilm}/(S_{total}*W_{\text{Fe minerals}}) = 0$$

$$\text{magnetite, } W_{mt} = S_{mt}/(S_{total}*W_{\text{Fe minerals}}) = 3.3$$

$$\text{hematite, } W_{hm} = S_{hm}/(S_{total}*W_{\text{Fe minerals}}) = 0.2$$

$$\text{nanophase oxide, } W_{npOx} = S_{npOx}/(S_{total}*W_{\text{Fe minerals}}) = 1.4$$

[61] **Acknowledgments.** Funding for Athena Science Team members was provided by NASA Mars Exploration Rover mission contracts through Cornell University and the Jet Propulsion Laboratory. Some of this work was carried out at and for JPL, California Institute of Technology, sponsored by NASA. G.K. acknowledges funding by the German Space Agency DLR under contracts 50QM9902 and 50QM0005.

References

Bandfield, J. L. (2002), Global mineral distributions on Mars, *J. Geophys. Res.*, *107*(E6), 5042, doi:10.1029/2001JE001510.

Bell, J. F., III, M. J. Wolff, P. B. James, R. T. Clancy, S. W. Lee, and L. J. Martin (1997), Mars surface mineralogy from Hubble Space Telescope imaging during 1994–1995: Observations, calibration, and initial results, *J. Geophys. Res.*, *102*, 9109–9123, doi:10.1029/96JE03990.

Bell, J. F., III, et al. (2000), Mineralogic and compositional properties of Martian soil and dust: Results from Mars Pathfinder, *J. Geophys. Res.*, *105*(E1), 1721–1755, doi:10.1029/1999JE001060.

Bell, J. F., III, et al. (2004a), Pancam multispectral imaging results from the Opportunity rover at Meridiani Planum, *Science*, *306*, 1703–1709, doi:10.1126/science.1105245.

Bell, J. F., III, et al. (2004b), Pancam multispectral imaging results from the Spirit Rover at Gusev Crater, *Science*, *305*, 800–806, doi:10.1126/science.1100175.

Bibring, J.-P., et al. (2005), Mars surface diversity as revealed by the OMEGA/Mars Express observations, *Science*, *307*, 1576–1581, doi:10.1126/science.1108806.

Christensen, P. R., et al. (2001), The Mars Global Surveyor Thermal Emission Spectrometer experiment: Investigation description and surface science results, *J. Geophys. Res.*, *106*, 23,823–23,872, doi:10.1029/2000JE001370.

Clark, B. C., et al. (2005), Chemistry and mineralogy of outcrops at Meridiani Planum, *Earth Planet. Sci. Lett.*, *240*, 73–94, doi:10.1016/jepsl.2005.09.040.

Clark, B. C., et al. (2007), Evidence for montmorillonite or its compositional equivalent in Columbia Hills, Mars, *J. Geophys. Res.*, *112*, E06S01, doi:10.1029/2006JE002756.

Day, J. M. D., L. A. Taylor, C. Floss, and H. Y. McSween (2006), Petrology and chemistry of MIL 03346 and its significance in understanding the petrogenesis of nakhlites on Mars, *Meteorit. Planet. Sci.*, *41*, 581–606.

Fegley, B., Jr., K. Lodders, A. H. Treiman, and G. Klingelhöfer (1995), The rate of pyrite decomposition on the surface of Venus, *Icarus*, *115*, 159–180, doi:10.1006/icar.1995.1086.

Gellert, R., et al. (2006), Alpha Particle X-ray Spectrometer (APXS): Results from Gusev Crater and calibration report, *J. Geophys. Res.*, *111*, E02S05, doi:10.1029/2005JE002555.

Glotch, T. D., et al. (2006), The mineralogy of the light-toned outcrop rock at Meridiani Planum as seen by the Minature Thermal Emission Spectrometer and implications for its formation, *J. Geophys. Res.*, *111*, E12S03, doi:10.1029/2005JE002672.

Guinness, E. A., R. E. Arvidson, M. A. Dale-Bannister, R. B. Singer, and E. A. Bruckenthal (1987), On the spectral reflectance properties of materials exposed at the Viking landing sites, *Proc. Lunar Planet. Sci. Conf. 17th*, Part 2, *J. Geophys. Res.*, *92*, suppl., E575–E587, doi:10.1029/JB092iB04p0E575.

Haskin, L. A., et al. (2005), Water alteration of rocks and soils on Mars at the Spirit rover site in Gusev Crater, *Nature*, *436*, 66–69, doi:10.1038/nature03640.

Hurowitz, J. A., S. M. McLennan, N. J. Tosca, and the Athena Science Team (2006), In situ and experimental evidence for acidic weathering of rocks and soil on Mars, *J. Geophys. Res.*, *111*, E02S19, doi:10.1029/2005JE002515.

King, P., and H. Y. McSween (2005), Effects of H_2O, pH, and oxidation state on the stability of Fe minerals on Mars, *J. Geophys. Res.*, *110*, E12S10, doi:10.1029/2005JE002482.

Le Bas, M. J., R. W. Le Maitre, A. Streckeisen, and B. Zanettin (1986), A chemical classification of volcanic rocks based on the total alkali-silica diagram, *J. Petrol.*, *27*, 745–750.

Li, R., et al. (2006), Rover localization and topographic mapping at the landing site of Gusev Crater, Mars, *J. Geophys. Res.*, *111*, E02S06, doi:10.1029/2005JE002483.

Lineberger, D. H., D. King, C. Shepard, S. Serafin, J. E. Moersch, and J. L. Bandfield (2006), Determination of olivine compositions from thermal infrared spectra, *Lunar Planet. Sci.*, *38th*, Abstract 2091.

McSween, H. Y., et al. (1999), Chemical, multispectral, and textural constraints on the composition and origin of rocks at the Mars Pathfinder landing site, *J. Geophys. Res.*, *104*(E4), 8679–8715, doi:10.1029/98JE02551.

McSween, H. Y., et al. (2004), Basaltic rocks analyzed by the Spirit rover in Gusev Crater, *Science*, *305*, 842–845, doi:10.1126/science.3050842.

McSween, H. Y., et al. (2006a), Alkaline volcanic rocks from the Columbia Hills, Gusev Crater, Mars, *J. Geophys. Res.*, *111*, E09S91, doi:10.1029/2006JE002698.

McSween, H. Y., et al. (2006b), Characterization and petrologic interpretation of olivine-rich basalts at Gusev Crater, Mars, *J. Geophys. Res.*, *111*, E02S10, doi:10.1029/2005JE002477.

Ming, D. W., et al. (2006), Geochemical and mineralogical indicators for aqueous processes in the Columbia Hills of Gusev Crater, Mars, *J. Geophys. Res.*, *111*, E02S12, doi:10.1029/2005JE002560.

Morris, R. V., D. C. Golden, J. F. Bell III, and H. V. Lauer Jr. (1995), Hematite, pyroxene, and phyllosicilicates on Mars: Implications from oxidized impact melt rocks from Maicouagan Crater, Quebec, Canada, *J. Geophys. Res.*, *100*(E3), 5319–5328, doi:10.1029/94JE01500.

Morris, R. V., et al. (2006a), Mössbauer mineralogy of rock, soil, and dust at Gusev Crater, Mars: Spirit's journey through weakly altered olivine basalt on the plains and pervasively altered basalt in the Columbia Hills, *J. Geophys. Res.*, *111*, E02S13, doi:10.1029/2005JE002584.

Morris, R. V., et al. (2006b), Mössbauer mineralogy of rock, soil, and dust at Meridiani Planum, Mars: Opportunity's journey across sulfate-rich outcrops, basaltic sand and dust, and hematite lag deposits, *J. Geophys. Res.*, *111*, E12S15, doi:10.1029/2006JE002791.

Morris, R. V., G. A. McKay, D. W. Ming, G. Klingelhofer, G. Schroder, C. Rodionov, and D. Yen (2006c), Magnetite in Martian meteorite MIL 03346 and Gusev Adirondack class basalt: Mössbauer evidence for variability in the oxidation state of Adirondack, *Lunar Planet. Sci.*, *37*, Abstract 1594.

Murchie, S., et al. (2007), First results from the Compact Reconnaissance Imaging Spectrometer for Mars (CRISM), *Lunar Planet. Sci.*, *38*, Abstract 1472.

Mustard, J. F., and J. M. Sunshine (1995), Seeing through the dust: Martian crustal heterogeneity and links to the SNC meteorites, *Science*, *267*, 1623–1626, doi:10.1126/science.7886449.

Ruff, S. W., et al. (2006), The rocks of Gusev Crater as viewed by the Mini-TES instrument, *J. Geophys. Res.*, *111*, E12S18, doi:10.1029/2006JE002747.

Squyres, S. W., and A. H. Knoll (2005), Sedimentary rocks at Meridiani Planum: Origin, diagenesis, and implications for life on Mars, *Earth Planet. Sci. Lett.*, *240*, 1–10, doi:10.1016/jepsl.2005.09.038.

Squyres, S. W., et al. (2003), Athena Mars rover science investigation, *J. Geophys. Res.*, *108*(E12), 8062, doi:10.1029/2003JE002121.

Squyres, S. W., et al. (2006), Rocks of the Columbia Hills, *J. Geophys. Res.*, *111*, E02S11, doi:10.1029/2005JE002562.

Squyres, S. W., et al. (2007), Pyroclastic activity at Home Plate in Gusev Crater, Mars, *Science*, *316*, 738–742, doi:10.1126/science.1139045.

Tosca, N. J., S. M. McLennan, D. H. Lindsley, and M. A. A. Schoonen (2004), Acid-sulfate weathering of synthetic Martian basalt: The acid fog model revisited, *J. Geophys. Res.*, *109*, E05003, doi:10.1029/2003JE002218.

Wang, A., et al. (2006), Evidence of phyllosilicates in Wooly Patch, an altered rock encountered at West Spur, Columbia Hills, by the Spirit rover in Gusev Crater, *J. Geophys. Res.*, *111*, E02S16, doi:10.1029/2005JE002516.

P. R. Christensen and S. W. Ruff, Department of Geological Sciences, Arizona State University, Tempe, AZ 85287, USA.

B. A. Cohen, NASA Marshall Space Flight Center, VP40, Huntsville, AL 35812, USA.

J. Crisp and A. Yen, Jet Propulsion Laboratory, California Institute of Technology, 4800 Oak Grove Drive, Pasadena, CA 91109, USA.

R. Gellert, Department of Physics, University of Guelph, MacNaughton Building, Gordon Street, Guelph, ON N1G2W1, Canada.

A. Ghosh, H. Y. McSween, and J. M. Moersch, Department of Earth and Planetary Sciences, University of Tennessee, 306 Geological Sciences Building, Knoxville, TN 37996-1410, USA. (mcsween@utk.edu)

G. Klingelhöfer and C. Schröder, Institut fur Anorganische und Analytische Chemie, Johannes Gutenberg-Universität, D-55128 Mainz, Germany.

T. J. McCoy, National Museum of Natural History, Smithsonian Institution, Washington, DC 20560-0119, USA.

R. V. Morris, NASA Johnson Space Center, Code KR, Houston, TX 77058-0000, USA.

A. D. Rogers, Division of Geological and Planetary Sciences, California Institute of Technology, MC 150-21, 1200 E. California Boulevard, Pasadena, CA 91125, USA.

S. W. Squyres, Department of Astronomy, Cornell University, 428 Space Sciences Building, Ithaca, NY 14853-0000, USA.